ARTICLE

**J. Cent. South Univ.** (2019) 26: 1530−1539
**DOI:** https://doi.org/10.1007/s11771-019-4109-4

Springer

# Lithium storage performance of {010}-faceted and [111]-faceted anatase $TiO_2$ nanocrystals

DU De-jian(杜德健)[1], DU Yi-en(杜意恩)[1, 2], YUE Wen-bo(岳文博)[1], YANG Xiao-jing(杨晓晶)[1]

1. Beijing Key Laboratory of Energy Conversion and Storage Materials, College of Chemistry, Beijing Normal University, Beijing 100875, China;
2. School of Chemistry & Chemical Engineering, Jinzhong University, Jinzhong 030619, China



**Abstract:** As a popular anode material for lithium-ion batteries, anatase $TiO_2$ nanoparticles with exposed {001} facets usually exhibit exceptional lithium storage performance owing to more accessible sites and fast migration of lithium ions along the good crystalline channels. However, there are few researches on the lithium storage capability of $TiO_2$ nanocrystals with other high-energy facets owing to lack of effective synthesis method for controlling crystal facets. Herein, anatase $TiO_2$ nanocrystals with exposed {010}- and [111]-facets are successfully prepared by using the delaminated tetratitanate nanoribbons as precursors. The electrochemical properties of these $TiO_2$ nanocrystals with high-energy surfaces and the comparison with commercial $TiO_2$ nanoparticles (P25) are studied. It is found that the cycle and rate performance of $TiO_2$ nanocrystals is highly improved by reducing the particle size of nanocrystals. Moreover, $TiO_2$ nanocrystals with exposed {010}- and [111]-facets exhibit better lithium storage capacities in comparison with P25 without a specific facet though P25 has smaller particle size than these $TiO_2$ nanocrystals, indicating that the exposed facets of $TiO_2$ nanocrystals have an important impact on their lithium storage capacity. Therefore, the synthesis design of high-performance $TiO_2$ materials applied in the next-generation secondary batteries should both consider the particle size and the exposed facets of nanocrystals.

**Key words:** titanium dioxide; nanocrystal; exposed facet; lithium-ion battery

**Cite this article as:** DU De-jian, DU Yi-en, YUE Wen-bo, YANG Xiao-jing. Lithium storage performance of {010}-faceted and [111]-faceted anatase $TiO_2$ nanocrystals [J]. Journal of Central South University, 2019, 26(6): 1530−1539. DOI: https://doi.org/10.1007/s11771-019-4109-4.

## 1 Introduction

As a popular n-type semiconductor electrode material, titanium dioxide ($TiO_2$) has been potentially applied in solar cells, sensors, sodium-ion batteries and lithium-ion batteries (LIBs) owing to its low cost, robust capability, good safety and environmental friendliness [1−3]. Moreover, the volume change of $TiO_2$ upon Li-ion intercalation and deintercalation is below 4%, which favors the safety and cycling stability of LIBs [4]. The insertion reaction of $Li^+$ into $TiO_2$ is expressed as follows: $TiO_2 + xLi^+ + xe^- \rightarrow Li_xTiO_2$ ($x \approx 0.5$), and this reaction is kinetically controlled by the solid-state diffusion of $Li^+$ [5]. Therefore, the crystal phase, particle size, morphology and surface structure of $TiO_2$ can significantly affect its

**Foundation item:** Projects(21573023, 51572031) supported by the National Natural Science Foundation of China; Project supported by the Grants-in-Acid for Doctor Research Funds; Project supported by "1331 Project" for Innovation Team Construction Plan Funds of Jinzhong University, China; Project supported by "1331 Project" for 2018 Key Innovation Team Construction Plan Funds of Shanxi Province, China

**Received date:** 2018-12-05; **Accepted date:** 2019-02-02

**Corresponding authors:** YUE Wen-bo, PhD, Professor; Tel: +86-10-58804229; E-mail: wbyue@bnu.edu.cn; ORCID: 0000-0003-3809-6733; YANG Xiao-jing, PhD, Professor; Tel: +86-10-58805476; E-mail: yang.xiaojing@bnu.edu.cn; ORCID: 0000-0003-3620-3507

electrochemical performance. For instance, the small particle size and high specific surface area of $TiO_2$ nanocrystals offer increased interfacial contact area with electrolyte and shorten the diffusion length for lithium ions, thereby highly enhancing the lithium storage capacity of $TiO_2$ [6−8]. Moreover, some recent reports indicate that the exposed planes of $TiO_2$ may also play an important part in lithium storage in nanostructured $TiO_2$ [9−13]. To date, anatase $TiO_2$ with exposed {001} facets has been widely studied due to its higher surface energy (0.90 J/m$^2$) in comparison with {101} and {010} facets (0.44 and 0.53 J/m$^2$) [14]. Compared to anatase $TiO_2$ with exposed {101} facets, anatase $TiO_2$ with exposed {001} facets exhibits superior lithium storage capability because of more accessible sites available and fast diffusion of lithium ions along the good crystalline channels (i.e., [001] direction) [9−13]. Moreover, a high Coulombic efficiency and remarkable capacity retention are also achieved for anatase $TiO_2$ with exposed {001} facets. However, there are few researches on the electrochemical properties of $TiO_2$ nanoparticles with other high-energy facets such as {010} facets so far [15].

Recently, Feng's group and our group cooperatively reported a novel synthesis of {010}-faceted and [111]-faceted anatase nanoparticles by using exfoliated tetratitanate nanoribbons as precursors [16, 17]. The particle sizes and the exposed facets of $TiO_2$ nanocrystals are easily controlled by changing pH values of solutions. Furthermore, it is interesting to find that the photocatalytic activities of these $TiO_2$ catalysts increase in the order of surface without a specific facet (commercial P25)<[111]-faceted surface< {010}-faceted surface, indicating a serious effect of the exposed facets on the photocatalytic properties of anatase $TiO_2$ [16]. It is reasonable that $TiO_2$ nanocrystals with various exposed facets would also exhibit different electrochemical performance. In this work, {010}-faceted and [111]-faceted anatase $TiO_2$ nanoparticles with various morphologies are prepared for studying the relationship between the exposed facets and the lithium storage property of $TiO_2$ nanocrystals. The results suggest that the crystalline phase, particle size, morphology and exposed facets are highly depended on the pH values of solutions. As a result, nanorod-shaped anatase $TiO_2$ nanocrystals with exposed [111]-facets are formed at pH 3, while rhombic-/cuboid-shaped and spindle-shaped anatase $TiO_2$ nanocrystals with expose {010}-facets are obtained at pH 5 and 7, respectively. To conveniently represent these $TiO_2$ nanocrystals, the samples are denoted as $TiO_2$-*T*, where *T* is the pH values (3, 5 and 7). The electrochemical tests indicate that $TiO_2$-3 exhibits better cycle and rate performance than $TiO_2$-5 and $TiO_2$-7 due to its small particle size. The large contact area between $TiO_2$-3 and electrolyte is favorable to the diffusion and intercalation of lithium ions. However, although P25 has smaller particle size than $TiO_2$-T, these anatase $TiO_2$ nanocrystals with exposed {010}- and [111]-facets still exhibit better lithium storage capacity than P25 without a specific facet. It is inferred that lithium ions are more facile to be attached to the high-energy facets of $TiO_2$ nanocrystals, resulting in the electrochemical performance improvement of $TiO_2$-T. Consequently, the electrochemical property of anatase $TiO_2$ can be remarkably increased by controlling not only the particle size and morphology, but also the exposed facets of $TiO_2$.

## 2 Experimental

### 2.1 Sample preparation

2.1.1 Tetratitanate nanoribbon

Potassium tetratitanate fibers ($K_2Ti_4O_9$) with layered structure were firstly immersed in 1 L of HCl solution (1 mol/L) with stirring for three days to obtain a protonated $H_2Ti_4O_9{\cdot}nH_2O$ (HTO) [16]. The acid exchange was repeated more than three times. The product was then collected by centrifugation and dried by vacuum freezing. The $TMA^+$-intercalated tetratitanate compound (TMA-HTO) was prepared by immersing the HTO sample (5.7 g) in tetramethylammonium hydroxide (TMAOH) solution (57 mL, 12.5%) and then calcination at 100 °C for 24 h. The as-synthesized TMA-HTO was dispersed in 570 mL of distilled water with stirring for 24 h. A colloidal suspension (exfoliated HTO) was collected after removing the large particles.

2.1.2 Anatase with various facets

The pH value of the colloidal solution was tuned to 3, 5 and 7 respectively by adding a HCl or TMAOH solution. The solutions (60 mL) with different pH were then transferred into a 100 mL Teflon-lined autoclave and heated at 170 °C for

24 h. After the autoclave was cooled down, $TiO_2$ nanocrystals were obtained after centrifugation and freeze-drying.

### 2.2 Sample characterization

Crystalline characterizations of samples were performed by X-ray diffraction (XRD) on a Phillips X'pert Pro MPD diffractometer. The morphologies and structures of samples were observed by scanning electron microscope (SEM) on a JEOL JSM-6700F with a voltage of 5 kV, transmission electron microscopy (TEM) and high-resolution TEM (HRTEM) on a JEOL JEM-2011 electron microscope with a voltage of 200 kV.

### 2.3 Electrochemical measurements

The electrochemical properties of samples were measured by using a LR2032-type coin cell. The negative electrode was Li metal and the positive electrode was a mixed slurry on a copper foil, including active materials (80%), super P carbon black (10%) and polyvinylidene difluoride (PVDF, 10%), and N-methyl-2-pyrrolidine (NMP) was used as solvent. 2.5 mg/cm$^2$ mass loading is necessary for active materials. The electrolyte was prepared by dissolving $LiPF_6$ (1 mol/L) in a mixed solution (EC:DEC:DMC with a 1:1:1 volume ratio). Coin cell was assembled in a glove box filled with Ar. Cyclic voltammetry and electrochemical impedance spectroscopy were tested on a Gamry Interface 1000 electrochemical station in the voltage range of 0.01−3.0 V (versus Li/Li$^+$) with a scan speed of 0.5 mV/s or with a frequency range of 100 kHz to 10 mHz, respectively. LAND test system was used to measure the galvanostatic charge–discharge performance in the voltage range of 0.01−3.0 V under a constant current of 0.05–1 A/g.

## 3 Results and discussion

### 3.1 Materials characterization

Anatase $TiO_2$ nanocrystals are prepared from as-synthesized HTO nanoribbons under hydrothermal treatment (see details in Section 2). According to our previous research, the crystalline phase (anatase single phase) is highly depended on the temperature (>150 °C) and pH (3−13) [16]. Herein, $TiO_2$ nanocrystals are prepared at 170 °C in solutions with pH of 3, 5 and 7, respectively. The XRD patterns of these $TiO_2$ nanocrystals are shown in Figure 1(a). All characteristic peaks in the XRD patterns are indexed into the tetragonal structure of anatase $TiO_2$. Moreover, it is found that the morphology of the nanocrystals is also influenced by the pH values. The SEM image of $TiO_2$-3 (Figure 1(b)) reveals that nanorod-like particles with an average size of about 60 nm in length and about 40 nm in width are formed at pH 3. At pH 5, two morphologies of $TiO_2$-5, cuboid and rhombic shapes, can be found in the SEM image (Figure 1(c)). The size of mainly cuboid particles is about 70 nm in length and about 55 nm in width. The morphology of $TiO_2$-7 changes to spindle shape when pH increases to 7 (Figure 1(d)), and the particle size increases to about 160 nm in length and about 55 nm in width. The particle size of these $TiO_2$ nanocrystals was analyzed by using Nano Measurer software. The histogram of particle length based on statistical results (Figures 2(a)−(c)) shows that the average size of $TiO_2$ nanocrystals is 58.8 nm for $TiO_2$-3, 69.8 nm for $TiO_2$-5 and 144.1 nm for $TiO_2$-7. This means that the crystalline size increases with the increase of pH values under the same condition. Our previous study indicates that the cracks in the precursor $[Ti_4O_9]^{2-}$ nanoribbons appear along the [010]-direction of the HTO below pH 3 and along [001]-direction above pH 7, leading to the different morphologies and particle sizes of anatase $TiO_2$ nanocrystals [16].

The morphologies and exposed facets of anatase $TiO_2$ nanocrystals were further studied by TEM. TEM images also confirm the formation of $TiO_2$ nanocrystals with a nanorod shape (Figure 3(a)), a cuboid or rhombic shape (Figure 3(c)) and a spindle shape (Figure 3(e)) respectively, which is in accord with the SEM observation. The nanocrystal in the HRTEM image of $TiO_2$-3 (Figure 3(b)) exhibits lattice spacings of 0.352 and 0.352 nm, which are assigned to the (101) and (011) planes of $TiO_2$ with an angle of ca. 82.1°. Therefore, the dominant exposed facets of $TiO_2$-3 are perpendicular to [111] crystal zone axis, and denoted as [111]-facets. In contrast, the lattice spacings of 0.351 and 0.473 nm in the HRTEM image of $TiO_2$-5 (Figure 3(d)) correspond to the (101) and (002) planes of $TiO_2$ with an angle of ca. 68.3°. Therefore, the dominant exposed facets of $TiO_2$-5 are the {010} facets and vertical to the [010] direction. The lattice spacings of 0.352 and

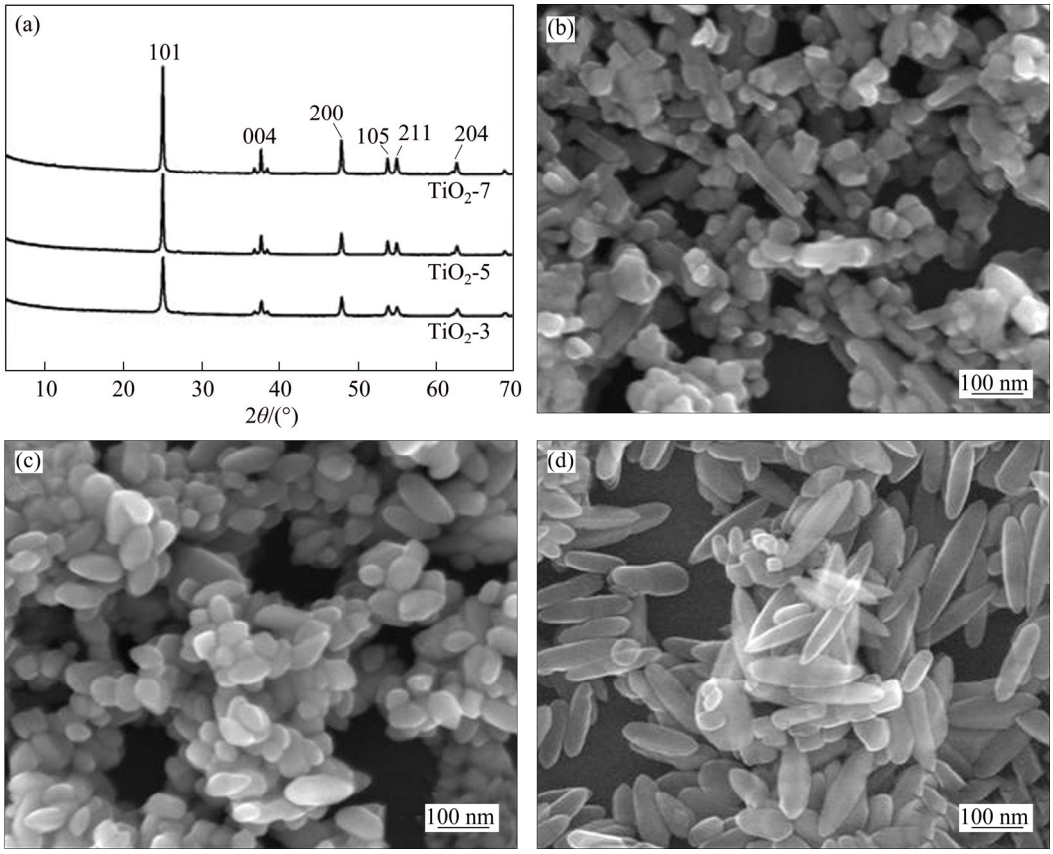


**Figure 1** XRD patterns of $TiO_2$-$T$ ($T$=3, 5, 7) (a) and corresponding SEM images of $TiO_2$-3 (b), $TiO_2$-5 (c) and $TiO_2$-7 (d)

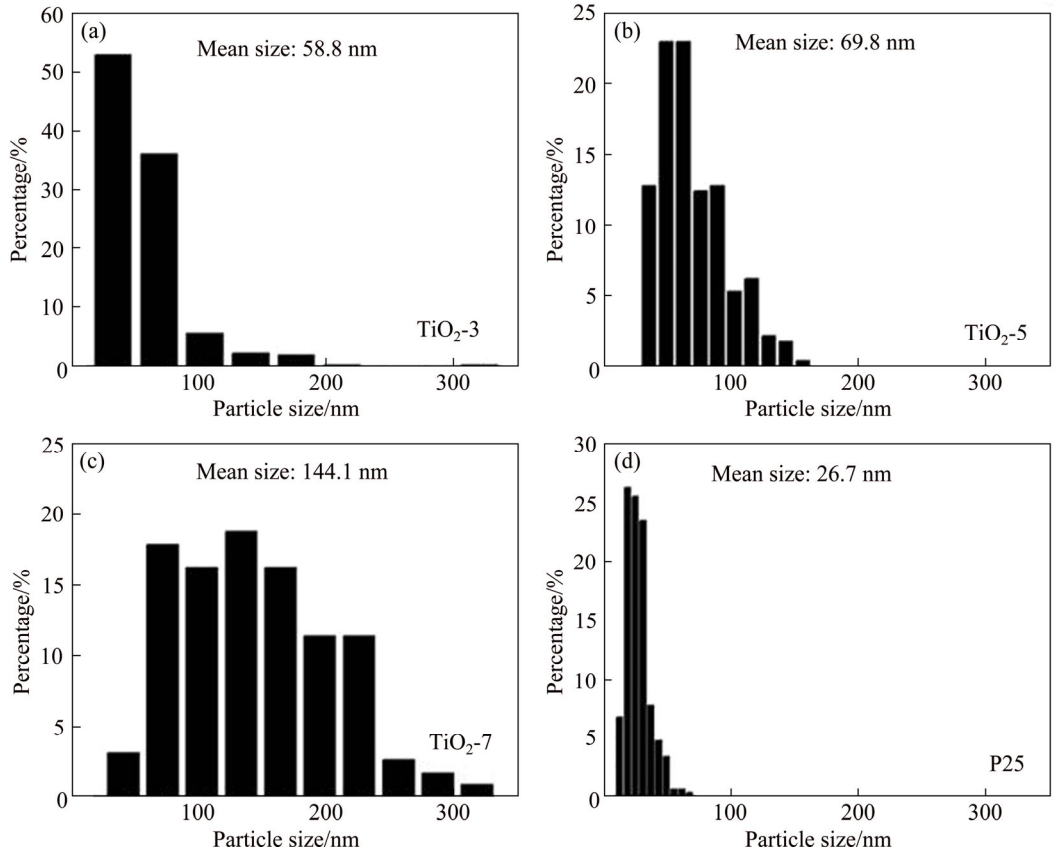


**Figure 2** Particle size distribution of $TiO_2$-3 (a), $TiO_2$-5 (b), $TiO_2$-7 (c) and P25 (d)

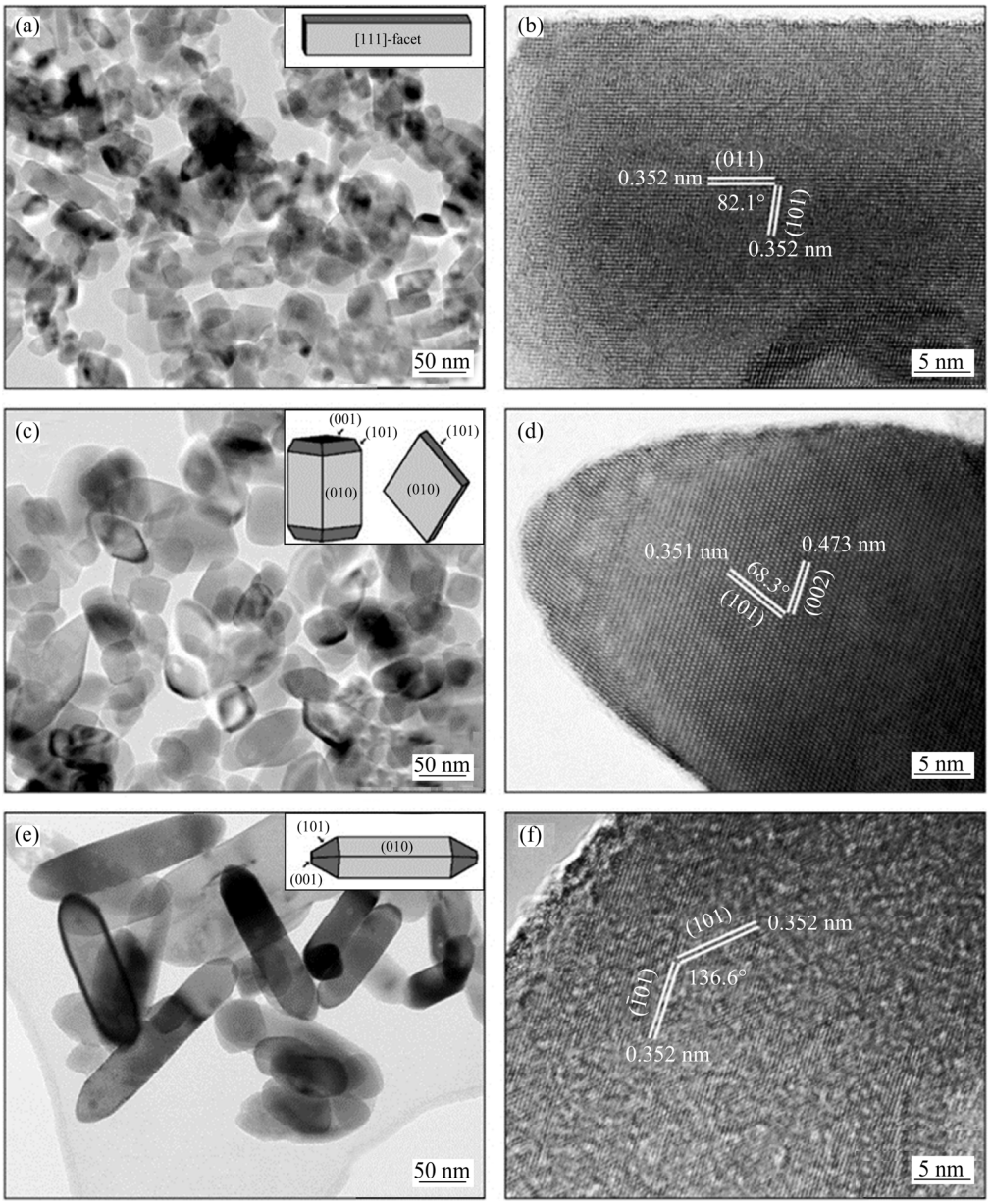


**Figure 3** TEM and HRTEM images of $TiO_2$-3 (a, b), $TiO_2$-5 (c, d) and $TiO_2$-7 (e, f) (Insets of (a, c, e) are structural models of $TiO_2$-3, $TiO_2$-5 and $TiO_2$-7, respectively)

0.352 nm in the HRTEM image of $TiO_2$-7 (Figure 3(f)) correspond to the (101) and ($\bar{1}$01) planes of $TiO_2$, and the angle between the two facets is 136.6°, also indicating that the {010} facets are the dominant exposed facets of $TiO_2$-7. In a word, nanorod-shaped $TiO_2$ nanoparticles with exposed [111]- facets were formed at pH 3, whereas rhombic-/cuboid- and spindle-shaped $TiO_2$ nanoparticles with exposed {010}-facets were formed at pH 5, and 7, respectively.

### 3.2 Electrochemical performance

The impact of the particle size and exposed facets on the electrochemical behaviors of anatase $TiO_2$ nanocrystals was studied by cyclic voltammetry and galvanostatic measurements. Figures 4(a), (c), (e) show the cyclic voltammograms (CVs) of $TiO_2$-3, $TiO_2$-5 and $TiO_2$-7 in the 1st, 2nd, 3rd and 6th cycles, respectively. There are two obvious cathodic and anodic peaks at about 1.5 and about 2.2 V, corresponding to the reversible transition from tetragonal anatase ($I4_1/amd$) to orthorhombic $Li_{0.5}TiO_2$ (*Imma*) [9, 12]. It is worth noting that the reduction and oxidation peaks still remain in the CV curves of $TiO_2$-3 after the first cycle, whereas these peaks become inapparent in the CV curves of $TiO_2$-5 and $TiO_2$-7 with the increase of cycle

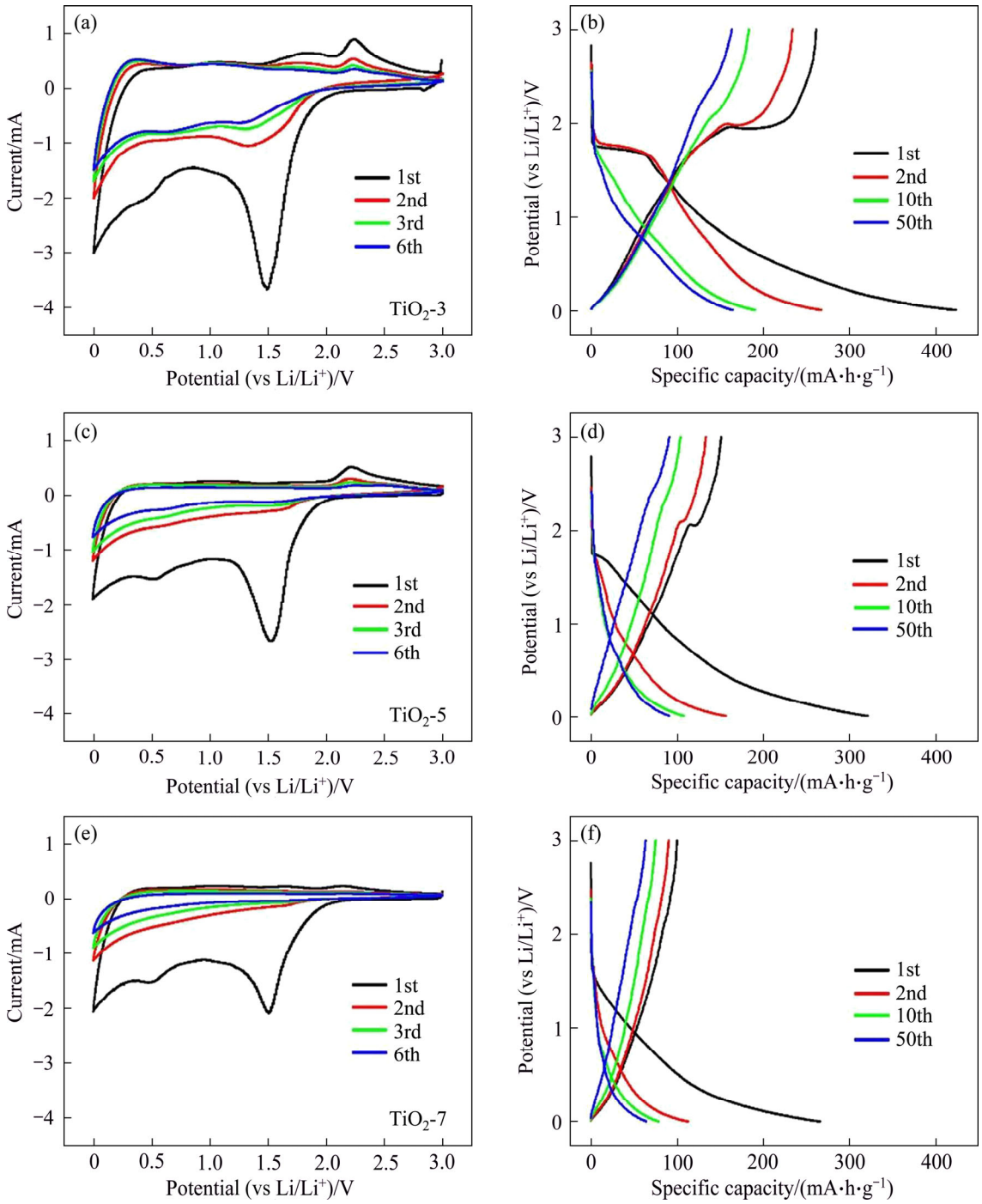


**Figure 4** CV curves (a, c, e) and voltage profiles (b, d, f): (a, b) $TiO_2$-3; (c, d) $TiO_2$-5; (e, f) $TiO_2$-7

number. The reduction peak at about 0.5 V is associated with the formation of solid electrolyte interface (SEI) films on the surface of $TiO_2$ nanocrystals [18, 19]. This peak would disappear as the SEI films become stable. Figures 4(b), (d), (f) depicts voltage profiles of these $TiO_2$ nanocrystals for the 1st, 2nd, 10th and 50th cycles. Two voltage plateaus at 1.7 and 2.1 V are observed in both charge and discharge curves of $TiO_2$-3. On the contrary, the voltage plateaus are not distinct in the charge/discharge curves of $TiO_2$-5 and $TiO_2$-7, which is well-matched with the CV results. It is inferred that lithium ions are more facile to be attached to the high-energy facets of $TiO_2$ nanocrystals, which is beneficial to the Li-ion intercalation and conversion reactions. In addition, according to the electrochemical properties of $TiO_2$-5 and $TiO_2$-7 with the same facets, the Li-ion intercalation performance is also influenced by the particle size, or in other words, the specific surface

area of $TiO_2$ nanocrystals.

The electrochemical properties of these $TiO_2$ nanocrystals are also measured, and $TiO_2$-3 shows the best cycle performance and rate capability among these $TiO_2$ nanocrystals (Figures 5(a), (b)). For instance, the reversible capacity of $TiO_2$-3 is maintained at about 160 mA h/g at 0.05 A/g over 100 cycles, which is comparable to the theoretical capacity of anatase $TiO_2$ (167.5 mA·h/g). On the contrary, $TiO_2$-5 and $TiO_2$-7 deliver the capacities of only about 90 and about 60 mA·h/g respectively over 100 cycles. The discharge capacity of $TiO_2$-3 is about 100 mA h/g as the current rate rises to 1 A/g, whereas the discharge capacities of $TiO_2$-5 and $TiO_2$-7 drop to about 60 and about 30 mA·h/g, respectively. The small particle size and large surface area of $TiO_2$-3 can enhance the electrolyte/electrode contact area and shorten lithium diffusion pathways, thereby improving the electrochemical performance of $TiO_2$-3. It should be noted that the increased contact area also causes a larger SEI film formed on $TiO_2$-3, which leads to more irreversible capacity losses and serious capacity fading in the initial cycles. The Coulombic efficiencies of $TiO_2$-3, $TiO_2$-5 and $TiO_2$-7 are 59.3%, 39.8% and 41.5% in the first cycle respectively, and reach to above 98% after the 10th cycle. The low initial Coulombic efficiencies are attributed to the formation of SEI films on $TiO_2$ nanocrystals and the irreversible generation of lithium titanate. It is interesting to note that $TiO_2$-3 has an abnormal higher initial Coulombic efficiency than $TiO_2$-5 and $TiO_2$-7, implying that the growth behavior of SEI film is totally different on different faceted crystals [19]. Accordingly, in addition to the particle size, the exposed facet also plays a significant part in the electrochemical properties of $TiO_2$ nanocrystals.

The electron and $Li^+$ transport in these $TiO_2$ nanocrystals were evaluated by using electrochemical impedance spectroscopy (EIS). Figure 5(c) shows the Nyquist plots consisting of a semicircle at the high frequency area, which is associated with the charge transfer resistance ($R_{ct}$), and a sloping straight line at the low frequency area, which is related to the diffusion performance of $Li^+$ ions in electrodes ($Z_w$) [20, 21]. The $R_{ct}$ values of samples were obtained after fitting curves with the equivalent circuit model (Figure 5(d)). The charge

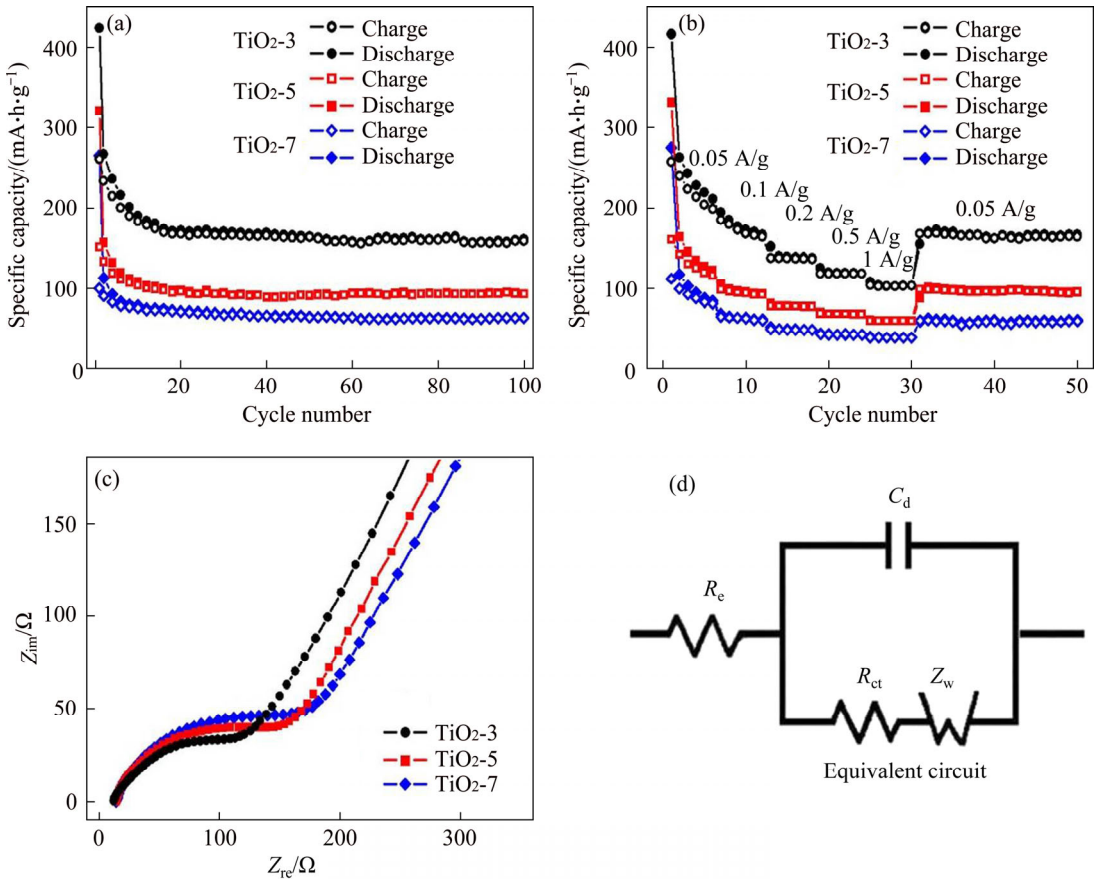


**Figure 5** Electrochemical properties of $TiO_2$-T: (a) Cycle performance at 0.05 A/g; (b) Rate performance at 0.05–1 A/g; (c) Electrochemical impedance spectra during 3 cycles; (d) Equivalent circuit used for fitting Nyquist curves

transfer resistance of $TiO_2$-3 is about 55.8 Ω, slightly lower than those of $TiO_2$-5 (about 78.6 Ω) and $TiO_2$-7 (about 87.1 Ω). The electron transfer relys on the magnitude of the band-gap, which is influenced by the particle size and defects of anatase [22]. More sub-band-gap states between the valence bands and conductions result in the lower charge-transfer resistance of $TiO_2$-3. Therefore, $TiO_2$-3 with lower resistance would display superior electrochemical performance as compared to other $TiO_2$ samples [23].

### 3.3 Comparison with P25

Besides the particle size, the high-energy facets of $TiO_2$ nanocrystals may also influence their electrochemical behavior. P25 is a well-known commercial $TiO_2$ powder containing about 80% anatase phase and 20% rutile phase (Figure 6(a)) [24]. SEM and TEM images (Figures 6(b) and (c)) reveal that P25 are mostly irregular spherical nanocrystals without a specific facet on the surface. In a typical HRTEM image of P25 (Figure 6(d)), the lattice spacings of 0.351 and 0.241 nm are assigned to the (101) and (004) planes of $TiO_2$ with an angle of ca. 68.3°, indicating the exposure of {010} facets on the basal plane. Furthermore, the (101) facets are parallel to the lateral faces of P25, indicating that the exposed facets are {101} on the lateral surface. The above results show that the small number of cuboid nanocrystals mainly expose {010} facets on the basal plane and {101} facets on the lateral surface. The main particle size of P25 is only 26.7 nm, much smaller than those of as-synthesized $TiO_2$ nanocrystals with exposed {010}- and [111]-facets (Figure 2D).

In theory, P25 should exhibit superior electrochemical performance than these $TiO_2$ nanocrystals due to its smaller particle size. However, the cycle and rate performance of P25 is merely comparable to those of $TiO_2$-7 (Figure 7), implying that the exposed facet serves as an important factor for the lithium storage capacity of $TiO_2$ as well. As reported previously, lithium ions prefer to be attached to the {010} facets of anatase rather than the {001} and {101} facets, and it is convenient for Li-ion transport along the [100] and [010] directions [25]. Therefore, $TiO_2$-5 with exposed {010}-facets exhibit slightly better electrochemical performance than P25 though $TiO_2$-5 has larger particle size. The [111]-facets are more complicated and their effects on the lithium transport need to be deeply studied in future.

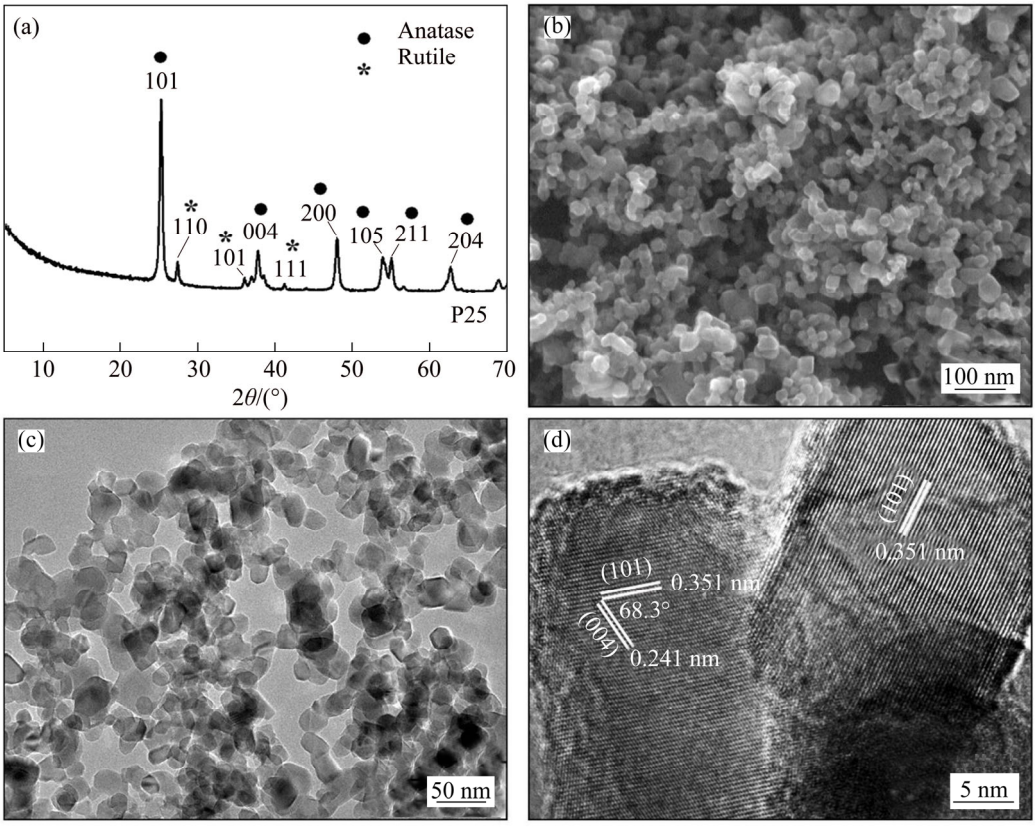


**Figure 6** XRD pattern (a), SEM (b), TEM (c) and HRTEM images (d) of P25

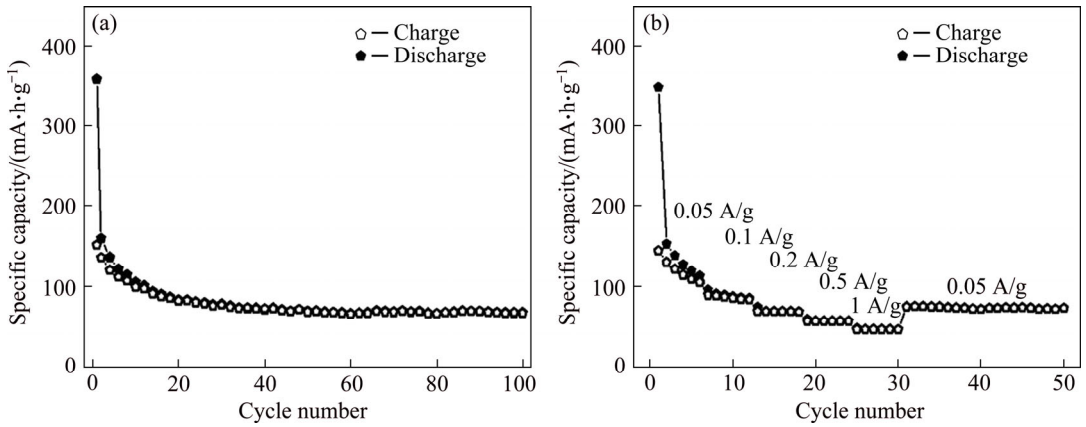


**Figure 7** Cycle performance of P25 at 0.05 A/g (a) and rate performance of P25 at 0.05–1 A/g (b)

## 4 Conclusions

Anatase $TiO_2$ nanocrystals with exposed {010}- and [111]-facets are successfully prepared by using exfoliated tetratitanate nanoribbons as precursors. The primary exposed facets of $TiO_2$ nanoparticles are controllable by adjusting the pH values of reaction solution. The cycle and rate performance of these $TiO_2$ nanocrystals are highly improved by reducing the particle size of nanocrystals. Moreover, these $TiO_2$ nanocrystals exhibit better electrochemical performance than P25 without a specific facet though P25 has smaller particle size. These results reveal that the electrochemical properties of anatase $TiO_2$ are affected not only by the crystal size and morphology, but also by the surface facets.

## References

[1] SUBRAMANIAN V, KARKI A, GNANASEKAR K I, EDDY F P, RAMBABU B. Nanocrystalline $TiO_2$ (anatase) for Li-ion batteries [J]. Journal of Power Sources, 2006, 159(1): 186−192. DOI: 10.1016/j.jpowsour.2006.04.027.

[2] HE Han-na, WANG Hai-yan, SUN Dan, SHAO Min-hua, HUANG Xiao-bing, TANG You-gen. N-doped rutile $TiO_2$/C with significantly enhanced Na storage capacity for Na-ion batteries [J]. Electrochimica Acta, 2017, 236: 43−52. DOI: 10.1016/j.electacta.2017.03.104.

[3] HE Han-na, SUN Dan, ZHANG Qi, FANG Fu, TANG You-gen, GUO Jun, SHAO Min-hua, WANG Hai-yan. Iron doped cauliflower-like rutile $TiO_2$ with superior sodium storage properties [J]. ACS Applied Materials & Interfaces, 2017, 9(7): 6093−6103. DOI: 10.1021/acsami.6b15516.

[4] DENG Da, KIM M G, LEE J Y, CHO J. Green energy storage materials: Nanostructured $TiO_2$ and Sn-based anodes for lithium-ion batteries [J]. Energy & Environmental Science, 2009, 2(8): 818−837. DOI: 10.1039/B823474D.

[5] KAVAN L. Lithium insertion into $TiO_2$ (anatase): electrochemistry, Raman spectroscopy, and isotope labeling [J]. Journal of Solid State Electrochemistry, 2014, 18(8): 2297−2306. DOI: 10.1007/s10008-014-2435-x.

[6] ARMSTRONG A R, ARMSTRONG G, CANALES J, BRUCE P G. $TiO_2$–B nanowires as negative electrodes for rechargeable lithium batteries [J]. Journal of Power Sources, 2005, 146(1, 2): 501−506. DOI: 10.1016/j.jpowsour.2005.03.057.

[7] ARMSTRONG G, ARMSTRONG A R, BRUCE P G, REALE P, SCROSATI B. $TiO_2$(B) nanowires as an improved anode material for lithium-ion batteries containing $LiFePO_4$ or $LiNi_{0.5}Mn_{1.5}O_4$ cathodes and a polymer electrolyte [J]. Advanced Materials, 2006, 18(19): 2597−2600. DOI: 10.1002/adma.200601232.

[8] SHI Si-qi, GAO Jian, LIU Yue, ZHAO Yan, WU Qu, JU Wang-wei, OUYANG Chu-ying, XIAO Rui-juan. Multi-scale computation methods: Their applications in lithium-ion battery research and development [J]. Chinese Physics B, 2016, 25(1): 018212. DOI: 10.1088/1674-1056/25/1/018212.

[9] CHEN Jun-song, TAN Yi-liang, LI Chang-ming, CHEAH Y L, LUAN De-yan, MADHAVI S, BOEY F Y C, ARCHER L A, LOU Xiong-wen, Constructing hierarchical spheres from large ultrathin anatase $TiO_2$ nanosheets with nearly 100% exposed (001) facets for fast reversible lithium storage [J]. Journal of the American Chemical Society, 2010, 132(17): 6124−6130. DOI: 10.1021/ja100102y.

[10] SUN Cheng-hua, YANG Xiao-hua, CHEN Jun-song, LI Zhen, LOU Xiong-wen, LI Chun-zhong, SMITH S C, LU Gao-qing, Yang Hua-gui. Higher charge/discharge rates of lithium-ions across engineered $TiO_2$ surfaces leads to enhanced battery performance [J]. Chemical Communications, 2010, 46(33): 6129−6131. DOI: 10.1039/C0CC00832J.

[11] YU Yan-long, WANG Xiao-liang, SUN Hong-yu, AHMAD M. 3D anatase $TiO_2$ hollow microspheres assembled with high-energy {001} facets for lithium-ion batteries [J]. RSC Advances, 2012, 2(20): 7901−7905. DOI: 10.1039/C2RA20718D.

[12] CHENG Xun-liang, HU Ming, HUANG R, JIANG Ji-sen, HF-free synthesis of anatase $TiO_2$ nanosheets with largely exposed and clean {001} facets and their enhanced rate

performance as anodes of lithium-ion battery [J]. ACS Applied Materials & Interfaces, 2014, 6(21): 19176−19183. DOI: 10.1021/am504971h.

[13] MING Hai, KUMAR P, YANG Wen-jing, FU Yu, MING Jun, KWAK W J, LI L J, SUN Y K, ZHENG Jun-wei, Green strategy to single crystalline anatase $TiO_2$ nanosheets with dominant (001) facets and its lithiation study toward sustainable cobalt-free lithium ion full battery [J]. ACS Sustainable Chemistry & Engineering, 2015, 3(12): 3086−3095. DOI: 10.1021/acssuschemeng.5b00553.

[14] XU Hua, REUNCHAN P, OUYANG Shu-xin, TONG Hua, UMEZAWA N, KAKO T, YE Jin-hua. Anatase $TiO_2$ single crystals exposed with high-reactive {111} facets toward efficient $H_2$ evolution [J]. Chemistry of Materials, 2013, 25(3): 405−411. DOI: 10.1021/cm303502b.

[15] HAN Xi-guang, HAN Xiao, SUN Lin-qiang, WANG Po, JIN Ming-shang, WANG Xiao-jun. Facile preparation of hybrid anatase/rutile $TiO_2$ nanorods with exposed (010) facets for lithium ion batteries [J]. Materials Chemistry and Physics, 2016, 171: 11−15. DOI: 10.1016/j.matchemphys.2015.11.048.

[16] DU Yi-en, FENG Qi, CHEN Chang-dong, TANAKA Y, YANG Xiao-jing. Photocatalytic and dye-sensitized solar cell performances of {010}-faceted and [111]-faceted anatase $TiO_2$ nanocrystals synthesized from tetratitanate nanoribbons [J]. ACS Applied Materials & Interfaces, 2014, 6(18): 16007−16019. DOI: 10.1021/am503914q.

[17] DU Yi-en, DU De-jian, FENG Qi, YANG Xiao-jing. Delithation, exfoliation, and transformation of rock-salt-structured $Li_2TiO_3$ to highly exposed {010}-faceted anatase [J]. ACS Applied Materials & Interfaces, 2015, 7(15): 7995−8004. DOI: 10.1021/acsami.5b00227.

[18] PFANZELT M, KUBIAK P, FLEISCHHAMMER M, WOHLFAHRT-MEHRENS M. $TiO_2$ rutile–An alternative anode material for safe lithium-ion batteries [J]. Journal of Power Sources, 2011, 196(16): 6815–6821. DOI: 10.1016/j.jpowsour.2010.09.109.

[19] ZHANG Qi, HE Han-na, HUANG Xiao-bing, YAN Jun, TANG You-gen, WANG Hai-yan. $TiO_2$@C nanosheets with highly exposed (001) facets as a high-capacity anode for Na-ion batteries [J]. Chemical Engineering Journal, 2018, 332: 57−65. DOI: 10.1016/j.cej.2017.09.044.

[20] ZHAO Peng, YUE Wen-bo, YUAN Xu, BAO Hua-ying. Exceptional lithium anodic performance of Pd-doped graphene-based $SnO_2$ nanocomposite [J]. Electrochimica Acta, 2017, 225: 322–329. DOI: 10.1016/j.electacta.2016.12.124.

[21] ZHANG Si-qi, LIN Rong, YUE Wen-bo, NIU Fang-zhou, MA Jie, YANG Xiao-jing. Novel synthesis of metal sulfides-loaded porous carbon as anode materials for lithium-ion batteries [J]. Chemical Engineering Journal, 2017, 314: 19−26. DOI: 10.1016/j.cej.2016.12.123.

[22] ABBASI A, MIRHABIBI A, ARABI H, GOLMOHAMMAD M, BRYDSON R. Synthesis, characterization and electrochemical performances of γ-$Fe_2O_3$ cathode material for Li-ion batteries [J]. Journal of Materials Science: Materials in Electronics, 2016, 27(8): 7953−7961. DOI: 10.1007/s10854-016-4788-7.

[23] XUE Xia, SUN Dan, ZENG Xian-guang, HUANG Xiao-bing, ZHANG He-he, TANG You-gen, WANG Hai-yan. Two-step carbon modification of $NaTi_2(PO_4)_3$ with improved sodium storage performance for Na-ion batteries [J]. Journal of Central South University, 2018, 25(10): 2320−2331. DOI: 10.1007/s11771-018-3916-3.

[24] CHEN Chang-dong, XU Lin-feng, SEWVANDI G A, KUSUNOSE T, TANAKA Y, NAKANISHI S, FENG Qi. Microwave-assisted topochemical conversion of layered titanate nanosheets to {010}-faceted anatase nanocrystals for high performance photocatalysts and dye-sensitized solar cells [J]. Crystal Growth & Design, 2014, 14(11): 5801−5811. DOI: 10.1021/cg501062r.

[25] YANG Xu-ming, WANG Chao, YANG Ying-chang, ZHANG Yan, JIA Xin-nan, CHEN Jun, JI Xiao-bo. Anatase $TiO_2$ nanocubes for fast and durable sodium ion battery anodes [J]. Journal of Materials Chemistry A, 2015, 3(16): 8800−8807. DOI: 10.1039/C5TA00614G.

**(Edited by FANG Jing-hua)**

## 中文导读

### 具有{010}和[111]晶面的锐钛矿型 $TiO_2$ 纳米晶体的储锂性能

**摘要：**作为锂离子电池的负极材料，具有{001}晶面的锐钛矿型 $TiO_2$ 纳米晶体通常展现出良好的储锂性能，这是由于该晶面具有更多的接触位点，同时锂离子沿着该晶格方向的扩散速度较快。然而，由于缺乏有效控制 $TiO_2$ 晶面的合成方法，对具有其它高能晶面 $TiO_2$ 晶体的储锂性能的研究较少。本文以剥离的钛酸盐纳米带为前驱体，通过水热法合成了具有{010}和[111]晶面的锐钛矿型 $TiO_2$ 纳米晶体。通过对该 $TiO_2$ 纳米晶体的电化学性能进行研究，并与商业用的 $TiO_2$ 纳米颗粒(P25)的性能进行比较，发现通过减小 $TiO_2$ 纳米晶的粒径，可以大幅度提高 $TiO_2$ 纳米晶体的循环和倍率性能。此外，尽管 P25 具有更小的粒径，相比没有特定晶面的 P25，具有{010}和[111]晶面的 $TiO_2$ 纳米晶体仍展现出更好的储锂能力。这表明 $TiO_2$ 纳米晶体的暴露晶面对其储锂性能同样具有重要影响。因此，在设计合成具有高性能的 $TiO_2$ 电极材料时，要同时考虑纳米晶体的粒径和暴露晶面等因素。

**关键词：**二氧化钛；纳米晶体；暴露晶面；锂离子电池